Smart Structures and Systems, Vol. 6, No. 7 (2010) 835-849
DOI: http://dx.doi.org/10.12989/sss.2010.6.7.835

Piezo-activated guided wave propagation and interaction with damage in tubular structures

Ye Lu[1,2], Lin Ye*[2,3], Dong Wang[2], Limin Zhou[3] and Li Cheng[3]

[1]State Key Laboratory of Mechanical System and Vibration, Shanghai Jiao Tong University, Shanghai 200240, People's Republic of China
[2]Laboratory of Smart Materials and Structures (LSMS), Centre for Advanced Materials Technology (CAMT), School of Aerospace, Mechanical and Mechatronic Engineering, The University of Sydney, NSW 2006, Australia
[3]Department of Mechanical Engineering, The Hong Kong Polytechnic University, Hong Kong SAR, China

(Received June 24, 2008, Accepted November 17, 2009)

Abstract. This study investigated propagation characteristics of piezo-activated guided waves in an aluminium rectangular-section tube for the purpose of damage identification. Changes in propagating velocity and amplitude of the first wave packet in acquired signals were observed in the frequency range from 50 to 250 kHz. The difference in guided wave propagation between rectangular- and circular-section tubes was examined using finite element simulation, demonstrating a great challenge in interpretation of guided wave signals in rectangular-section tubes. An active sensor network, consisting of nine PZT elements bonded on different surfaces of the tube, was configured to collect the wave signals scattered from through-thickness holes of different diameters. It was found that guided waves were capable of propagating across the sharp tube curvatures while retaining sensitivity to damage, even that not located on the surfaces where actuators/sensors were attached. Signal correlation between the intact and damaged structures was evaluated with the assistance of a concept of digital damage fingerprints (DDFs). The probability of the presence of damage on the unfolded tube surface was thus obtained, by which means the position of damage was identified with good accuracy.

Keywords: guided waves; damage identification; tubular structures; active sensor networks; piezoelectric element.

1. Introduction

Novel methods of damage identification based on guided wave propagation have been the subject of research since the 1980s. Guided waves, which generally exist on structural surfaces (Rayleigh waves) or in plate-like structures (Lamb waves), can propagate over a relatively long distance, and thus allow a broad area or a whole section of a structure to be interrogated with only a few transducers. Guided wave-based approaches have been successful in identifying various types of damage in complex engineering structures, such as composite structures (Thwaites and Clark 1995, Castaings and Hosten 2001, Zhou *et al*. 2007), aircraft fuselage structures/components (Dalton *et al*. 2001, Grondel *et al*. 2002, Giurgiutiu *et al*. 2003, Monnier 2006) and civil infrastructure (Pu *et al*. 2004, Rizzo and Lanza di Scalea 2006). It has well been substantiated that guided waves can propagate not only in curved geometries but also in sections of a structure that are otherwise inaccessible, locating some previously undetectable faults (Castaings and Hosten 2001).

*Corresponding Author, Professor, E-mail: lin.ye@sydney.edu.au

Tubular structures are widely used in infrastructure applications, e.g., as railway and bridge components and sections. A train bogie frame, for instance, which is commonly unobserved by passengers, generally consists of two side beams and two cross beams formed into an H-shaped frame, where all beams are close tubular sections with internal vertical ribs. Integrity assessment of these components is essential for the safety of the structures. Such assessment, however, is intricate because of the complex geometry and, at times, inaccessibility of the components. Nevertheless, it has been shown that guided waves can propagate along any desired helical path from circumferential to longitudinal, or throughout the thickness of a circular-section pipe wall, by virtue of different modes (Alleyne *et al.* 2001, Demma *et al.* 2003, 2004). On the basis of such advantages, guided waves have demonstrated potential for identifying damage on the inner or outer surface of a circular-section pipe, including erosion/corrosion (Cawley and Alleyne 1996, Pei *et al.* 1996, Leonard and Hinders 2003), crack/notch (Lowe *et al.* 1998, Lowe 1998, Valle *et al.* 2001, Demma *et al.* 2004, Tua *et al.* 2005) and hole (Park *et al.* 1996).

On the other hand, as well as difficulties due to the inherent properties of guided waves, e.g., dispersion, attenuation and complex boundary reflection, guided wave modes in tubular structures are generally complicated by extra modes with harmonic variation of displacements and stresses around the circumference (Lowe *et al.* 1998). Between one actuator-sensor pair many helical routes can exist so that, in addition to the waves propagating along the shortest route between actuator and sensor, other propagation manners of waves are also available (Leonard and Hinders 2003). As a result, some waves along routes with a steeper helical path travel further around the tube circumferentially and may miss the sensor, whereas others travel one or more complete loops around the tube and then arrive at the sensor. Moreover, helical waves can be generated in both clockwise and counter-clockwise directions, depending on the relative angular positions of the actuator and sensor. With the occurrence of damage, the aforementioned phenomena become even more complex as the damage scatters the waves and causes possible mode conversion.

Irregular tubular structures (with non-circular cross-sections) are expected to create additional complexities for wave propagation because of the steeper curvature at corners. In comparison with circular-section pipes, the rectangular-section tube may therefore cause greater difficulty for interpretation of guided wave propagation across the tube surfaces. In this study, the propagation characteristics of piezo-activated guided waves in an aluminium rectangular-section tube are investigated. An active sensor network consisting of nine PZT elements bonded on different surfaces of the tube is configured to collect guided wave signals scattered from through-thickness holes of different diameters. The probability of the presence of damage in the unfolded tube surface is obtained using signal correlation between the intact and damaged structures, based on a concept of digital damage fingerprints (DDFs), pinpointing the location of damage.

2. Guided wave modes in pipes

Guided wave modes in circular-section pipes can be generally labelled L(0, n), T(0, n) and F(m, n), respectively, referring to longitudinal, torsional and flexural modes, where m is the harmonic number of circumference variation and n represents the order of wave modes, as in the notation for plate waves (Demma *et al.* 2004). The longitudinal and torsional modes are axis-symmetrical modes whereas the flexural modes are non-symmetrical (Rose 1999). In general, guided waves propagate in a pipe as longitudinal, torsional or flexural modes separately at low frequencies, whereas at higher frequencies guided waves behave to a greater extent like those in a curved plate or shell, i.e., Lamb wave modes. However, there is no distinct separation between these two group modes and all wave modes may exist synchronously and be intermingled with each other (Leonard and Hinders 2003). In particular, L(0,1) can be regarded as the fundamental anti-symmetrical Lamb wave mode (A_0), while L(0,2) shows similar properties to the fundamental symmetrical Lamb wave mode (S_0) (Silk and Bainton 1979).

For wave excitation, longitudinal modes, mainly L(0,1) and L(0,2) modes, are usually preferable to flexural modes because of the axis-symmetrical property that enables an inspection of 360° along the circumference of pipes (Rose 1999, Tua *et al.* 2005). Non-symmetrical modes have also been used for damage detection in pipes after appropriate mode tuning (Zhang *et al.* 2006). Recently, the fundamental torsional mode T(0,1) has been employed as well to evaluate damage in the form of cracks and notches in pipes, based on the advantage that the mode shape of T(0,1) is frequency-independent and therefore it is completely non-dispersive, with the same velocity value as that of bulk shear waves (Demma *et al*. 2003).

3. Experiment configuration

An aluminium alloy rectangular-section tube was selected for this study, with the dimensions and properties listed in Table 1. Three small PZT elements (PI® PIC151) with the properties listed in Table 2 were bonded at the central line of the top surface (Fig. 1(a)) using an adhesive epoxy. Six more PZT elements of the same size and properties were bonded at similar positions along one side and the bottom surfaces of the tube, illustrated in an unfolded configuration in Fig. 1(b), where the sensors are denoted as S1 to S9. Each sensor could both activate and sense guided wave signals, functioning as an active sensor network. The wiring of the sensors was completed using shielded cables to reduce cross-interference and other environmental noise. The two longitudinal ends of the tube were fixed onto the platform of a Newport RS4000 stabilizer (damping table) using metal screws.

The digital signal was programmed and actuated by an Agilent® E1441 arbitrary waveform generator. After being converted by a built-in D/A converter and amplified by a piezo system amplifier (EPA-104), the analog signal imposed an electric field on the PZT actuator, with a peak-to-peak voltage of

Table 1 Geometry and mechanical properties of the aluminium tube

Geometry (mm)	Length: 500, width: 63, height: 38, thickness: 3.2
Density ρ_{al} (kg/m^3)	2700
Poisson's ratio υ_{al}	0.33
Young's modulus E_{al} (GPa)	71

Table 2 Mechanical properties of piezoelectric elements

Geometry (mm)	Length: 20, width: 5, thickness: 1
Density ρ_p (g/cm^3)	7.80
Poisson's ratio υ_p	0.34
Charge constant d_{31} (m/V)	-210×10^{-12}
Charge constant d_{33} (m/V)	500×10^{-12}
Young's modulus E_p (GPa)	100

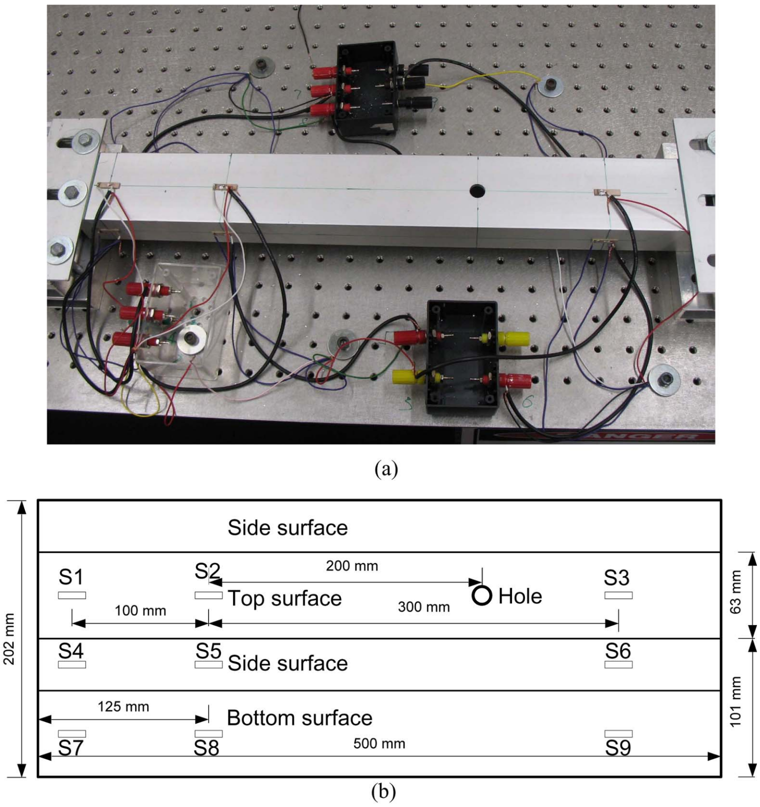

Fig. 1 Aluminium tube with PZT elements in experiments: (a) experimental set-up and (b) configuration and dimensions

35 V. Dual-channel synchronous signal acquisition was performed on individual PZT sensors by a digitizer (Agilent® E1437A) through the IEEE-488 bus, at a sampling rate of 20.48 MHz. Because of the incompatibility between the sensor output and acquisition hardware (from analog to digital signals), a signal conditioner (Agilent® E3242A) was used to condition the signal and complete the functions of amplification, de-noising, electrical isolation and multiplexing, before the signal was acquired by the digitizer.

Signal excitation and acquisition were performed on the Agilent® VXI signal simulation/acquisition platform. The supportive software was developed on NI Labview® (Version: 5.6, National Instrument Co.), Matlab® (Version 6.3, Mathworks Inc.) and HP VEE® (Version: 4.0, Hewlett-Packard Co.) platforms to fulfill the designed functionalities, with the aid of Agilent® virtual instrument software architecture (VISA) and Agilent® standard instrument control library (SICL).

4. Guided waves in rectangular-section tubes

4.1 Selection of optimal excitation frequency

Considering the tube thickness (3.2 mm in this study), the excitation frequency for guided waves

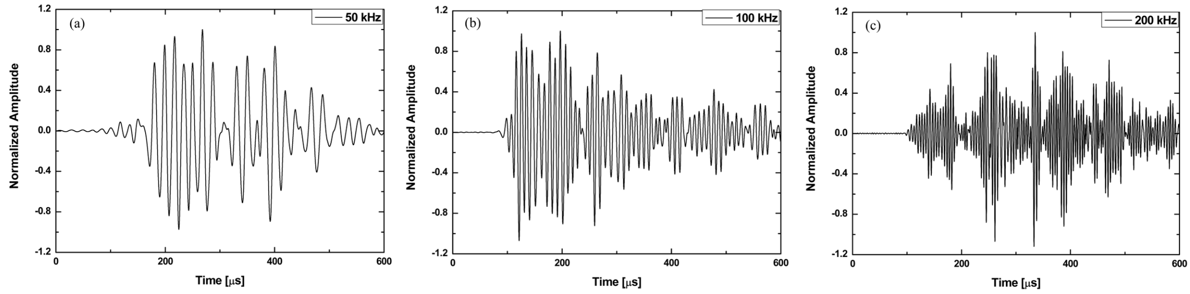

Fig. 2 Comparison of PZT-activated guided waves at different excitation frequencies: (a) 50 kHz, (b) 100 kHz and (c) 200 kHz

had to be correspondingly defined so as to avoid the emergence of multiple high order wave modes with complex waveforms (Hesse and Cawley 2006). On the other hand, poor time resolution and large wavelength of guided waves at lower frequencies make signal interpretation more difficult because of the low sensitivity to minute damage. Therefore, the excitation frequency for guided waves was first optimized before the subsequent damage identification.

Propagation properties of guided waves at a central frequency from 50 to 250 kHz were evaluated when a five-cycle toneburst modulated with a Hanning window was applied to the actuator. Typical wave signals from the actuator-sensor pair of S2-S3 acquired at frequencies of 50, 100 and 200 kHz are plotted in Figs. 2(a)-(c), respectively. It is evident that the waveforms are significantly different from each other, especially with regard to the arrival time and amplitude of the first wave packet. A Hilbert transform (Diligent *et al*. 2002) was adopted to obtain the energy envelope for monitoring changes in amplitude of wave packets. After normalization by the value at the frequency of 100 kHz, the amplitudes of the first wave packet at different excitation frequencies are compared in Fig. 3, as well as the changes in corresponding group velocity in the frequency range of interest. It is evident that the propagating velocity of the investigated wave mode is dependent on the frequency, and it reaches a plateau around 5300 m/s (Fig. 3(a)), whereas the magnitude increases with frequency and reaches a peak value around 100 kHz, but starts to decrease when the excitation frequency increases further (Fig. 3(b)).

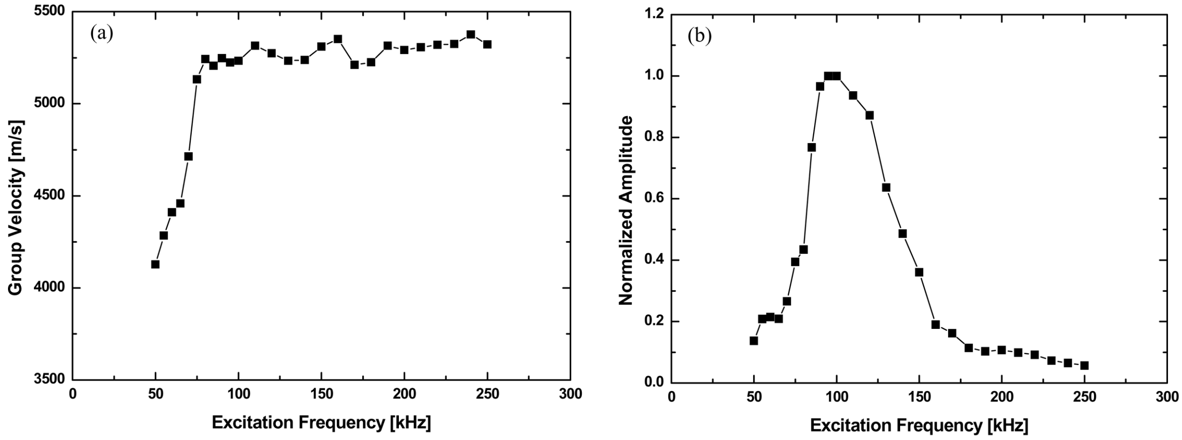

Fig. 3 Performance of the first wave packet in terms of (a) propagating velocity and (b) amplitude

On the analogy of guided waves propagating in circular-section pipes (Demma *et al*. 2004), the observed wave mode is recognized as L(0,2) which emerges with a marginal but increasing amplitude after the cut-off frequency. After a rapid change in propagating velocity, it gradually evolves into a less dispersive range with a relatively constant group velocity. These properties are distinct from the S_0 mode propagating in plate-like structures, although both modes demonstrate mainly in-plane vibration. On the other hand, the reason for the significant decrease in the amplitude of L(0,2) mode after 100 kHz is that guided waves in tubular structures may gradually develop into plate (Lamb) wave modes at relatively higher frequencies, where dominance of the S_0 mode in the wave signals (similar to L(0,2)) is lost (Giurgiutiu and Cuc 2005, Tua *et al*. 2005). Another possible reason for the maximal magnitude at an excitation frequency of 100 kHz is attributed to the fact that the characteristic length of PZT selected for actuators and sensors is 20 mm, which is close to half the wavelength of L(0,2) mode at 100 kHz. Such a configuration proves effective for achieving maximal magnitude of guided waves excited and captured by PZT elements (Lanza di Scalea *et al*. 2007). As a result of these observations, subsequent investigations in this study were conducted at the excitation frequency of 100 kHz, where L(0,2) mode demonstrated good wave behaviour.

4.2 Propagation mechanisms

It is appreciated that rectangular-section tubes may induce additional mechanisms for wave propagation in comparison with their circular-section counterparts because of the steeper curvature at corners. In this study, two three-dimensional FEM (finite element method) models were created on the PATRAN® platform using eight-node brick solid elements, one for a rectangular-section tube and the other for a circular-section one with an equivalent outer radius (32.2 mm), shown in Figs. 4(a) and (b), respectively. The element size in the surface plane was set to be 1 mm, and four layers were modelled through the thickness (3.2 mm) to maintain a ratio of 1.25. Dynamic simulation was accomplished using ABAQUS/EXPLICIT® code (Lu *et al*. 2007). An in-plane 5-cycle shear force at a central frequency of 100 kHz modulated with a Hanning window was applied to the nodes at the periphery of the actuator, based on a model of the actuator attached on the plate surface (Lu *et al*. 2007); the element responses at the positions of sensors were acquired, calibrated with the output voltage of a PZT sensor (Lu *et al*. 2007). The sampling frequency was selected as 20.48 MHz, consistent with the experimental settings.

Figs. 5(a)-(c) compare wave signals captured by sensors S2, S5 and S9, respectively, which were located on different surfaces of the rectangular- and circular-section tubes, when sensor S1 acted as the actuator. It is noted that the waveforms are different in the two cases, although the guided waves

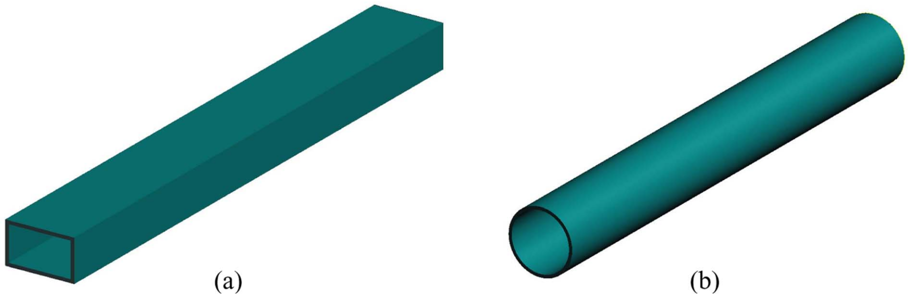

(a) (b)

Fig. 4 Geometric models for (a) rectangular-section tube and (b) equivalent circular-section tube in FEM simulations

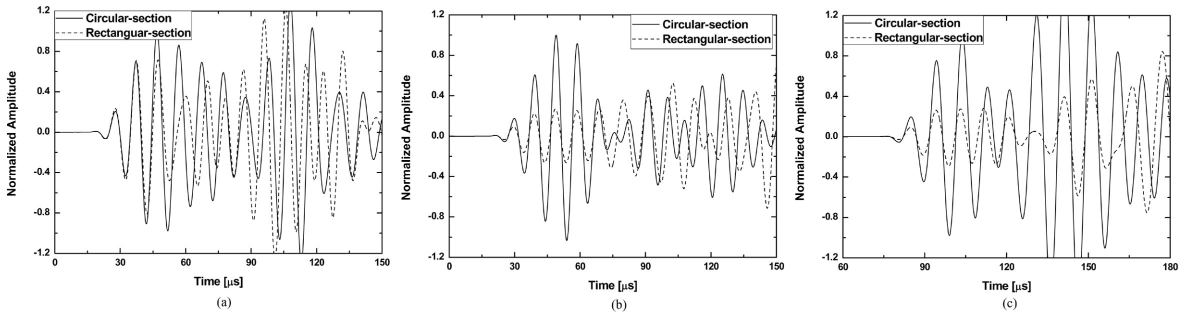

Fig. 5 Captured wave signals in rectangular- and circular-section tubes: (a) sensor S2, (b) sensor S5 and (c) sensor S9

arrive at the same time for the same propagation distance. In particular, the magnitudes of the guided waves propagating along the surface of the rectangular-section tube were significantly lower than those for the circular-section tube, indicating more energy loss when guided waves propagated in the rectangular-section tube. The significant energy loss would inevitably increase the complexity of signal processing and subsequent damage identification because of the weak signals.

5. Interaction with damage

A hole of 3 mm diameter was introduced by drilling at the central line at a distance of 325 mm from the left end of the pipe, and the diameter of the hole was subsequently enlarged step-by-step to 4.6 mm, 9.0 mm, 10.5 mm and 11.9 mm (Fig. 1). The interactions between guided waves and the damage of five different diameters were studied in experiments, with the assistance of the active sensor network. Sensors S1, S4 and S7 were activated to generate guided waves respectively to investigate the capability of guided waves for effective damage identification in cases where (1) the damage was located on the same surface as the actuator and the sensor; (2) the damage and the actuator only were located on the same surface; and (3) the damage was not located on the same surface as the actuator and the sensor.

For case 1, where sensor S1 functioned as the actuator, the normalized signals received at sensors S2 (for normal wave reflection from the damage) and S3 (for normal wave transmission from the damage) for the intact structure (benchmark) and for the tube with a hole of 11.9 mm diameter are compared in Figs. 6(a) and (b), respectively. The differences in the signals captured by sensor S2 are clearly visible although the reflected waves from the damage cannot be identified exclusively because of the overlap with other wave components existing in the benchmark signal. In addition, it is observed that the amplitude of the transmitted wave signal decreases in the damaged tube in comparison with the benchmark signal.

Damage-scattered wave signals were also collected by sensors S5, S6, S8 and S9 when sensor S1 was activated, for the purpose of simulating the case where only the damage and the actuator are located on the same surface (case 2). Figs. 6(c) and (d) illustrate the captured signals at sensors S6 and S9, respectively, for the benchmark and the tube with a hole of 11.9 mm diameter. It can be observed that the signal discrepancy between the tubes with and without hole damage is still visible, implying that guided waves are capable of propagating across the sharp curvature of the rectangular-section tube while maintaining sensitivity to damage that is not located on the surfaces where the

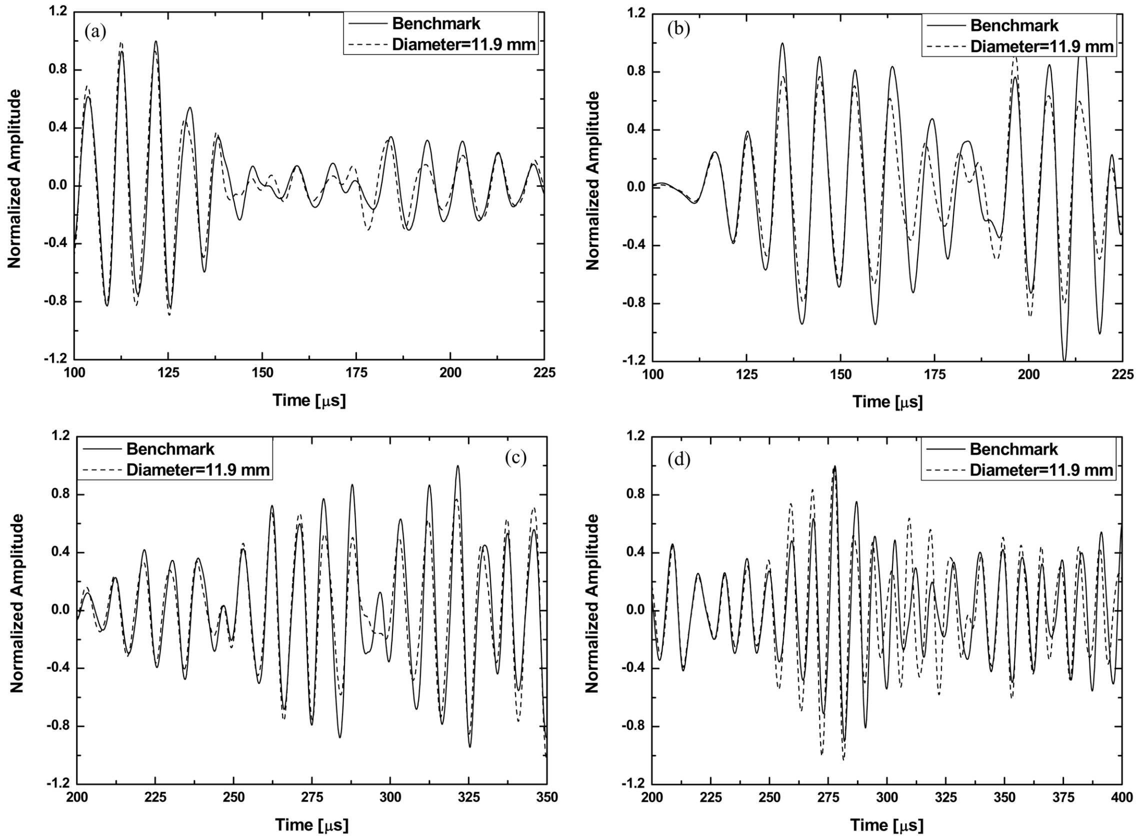

Fig. 6 Captured wave signals with and without a hole of 11.9 mm diameter with S1 as actuator: (a) sensor S2, (b) sensor S3, (c) sensor S6 and (d) sensor S9

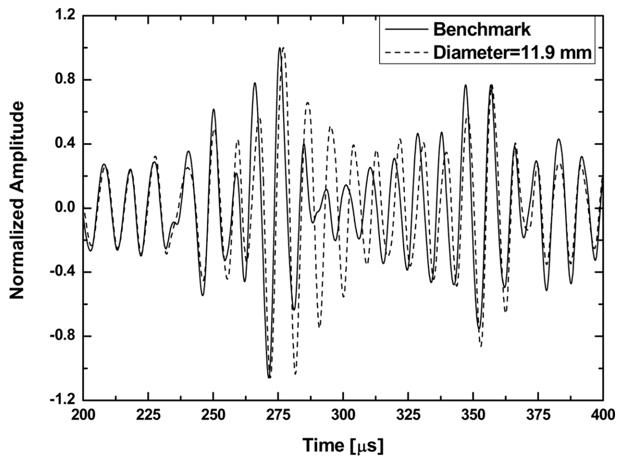

Fig. 7 Wave signals from sensor S6 with and without a hole of 11.9 mm diameter with S4 as actuator

sensors are attached.

To monitor wave scattering from a hole that was not located on the surface of the actuator and the sensor (case 3), sensors S4 and S7 were activated separately, and sensors S5, S6 and S8, S9 were

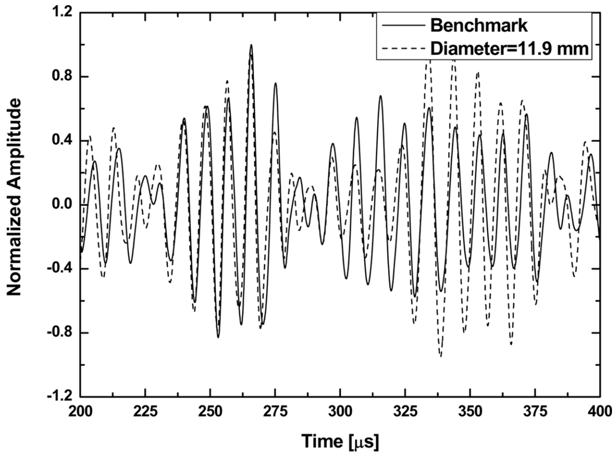

Fig. 8 Wave signals from sensor S9 with and without a hole of 11.9 mm diameter with S7 as actuator

correspondingly deployed as receivers. Typical signals captured by sensors S6 (with S4 as the actuator) and S9 (with S7 as the actuator) are plotted in Figs. 7 and 8, respectively, where the sensors still exhibit noticeable sensitivity to the hole damage. From Figs. 6-8, it is substantiated that guided wave components scattered by the damage could propagate across the sharp structural curvature, and they could be captured by sensors that were not located on the surface where the damage occurred. It can be concluded by cases 1-3 that PZT-activated guided waves show promising potential to effectively detect damage at an arbitrary location in tubular structures. In particular, for the circumstance where a structure or part of it under inspection is inaccessible, the sensors can be configured and installed on one surface of the structure only, but can still monitor the integrity of the structure.

On the other hand, it is evident that the captured wave signals are too complex to be processed for quantitative assessment with a normal forward analysis in which the reflection or transmission coefficient can be quantitatively obtained after a Hilbert transform (Lu *et al*. 2007, 2008). In detail, the scattered waves (including reflected and transmitted waves) induced by the presence of the hole damage overlap with other incident wave modes at lower propagating velocities and/or with the fast reflections of L(0,2) mode from the nearest structural boundaries. It is thus difficult to define the exact time-of-flight (ToF) of wave components scattered by the damage to determine its position. An algorithm based on signal correlation is therefore developed in this study, by means of which the probability of the existence of damage in the inspected structure can be obtained.

6. Probability of presence of damage

It is appreciated that the probability of the existence of damage at a particular point in the structure can be determined by the correlation coefficient, which represents the severity of the signal change in actuator-sensor pairs, and the relative position from the point to these pairs (Hay *et al*. 2006). Assuming that a total of N actuator-sensor pairs in an active sensor network are involved for constructing the probability of the existence of damage, the probability of damage $P(x, y)$ at position (x, y) can be expressed as (Hay *et al*. 2006, Zhao *et al*. 2007).

$$P(x,y)=\sum_{k=1}^{N}(1-\rho_k)\left(\frac{-1}{\beta-1}\bullet R(x,y,x_{ak},y_{ak},x_{sk},y_{sk})+\frac{\beta}{\beta-1}\right) \tag{1}$$

$$R(x, y, x_{ak}, y_{ak}, x_{sk}, y_{sk}) = \begin{cases} R_c(x, y, x_{ak}, y_{ak}, x_{sk}, y_{sk}), & R_c(x, y, x_{ak}, y_{ak}, x_{sk}, y_{sk}) < \beta \\ \beta, & R_c(x, y, x_{ak}, y_{ak}, x_{sk}, y_{sk}) \geq \beta \end{cases} \tag{2}$$

where

$$R_c(x, y, x_{ak}, y_{ak}, x_{sk}, y_{sk}) = \frac{\sqrt{(x - x_{ak})^2 + (y - y_{ak})^2} + \sqrt{(x - x_{sk})^2 + (y - y_{sk})^2}}{\sqrt{(x_{ak} - x_{sk})^2 + (y_{ak} - y_{sk})^2}}$$

is the ratio of the sum of the distances from point (x, y) to actuator (x_{ak}, y_{ak}) and sensor (x_{sk}, y_{sk}) to the distance between the corresponding actuator and sensor. ρ_k is the correlation coefficient between signals for the damaged and benchmark structures of the k^{th} actuator-sensor pair. β is a scaling parameter controlling the area influenced by the k^{th} actuator-sensor pair, and was set to 1.03 in this study (Hay *et al*. 2006). Eq. (1) indicates that the lower the values of coefficient ρ_k and ratio R, the higher the probability of the presence of damage at a specific point of the structure.

The approach based on signal correlation has been successfully applied for plate-like structures to identify material loss (Hay *et al*. 2006), hole (Lu *et al*. 2009) and multiple notches (Wang *et al*. 2009), respectively. However, the captured signals in tubular structures are in fact the combination of guided waves propagating in both clockwise and counter-clockwise helical paths, unlike the propagation manner in plate-like structures. As a result, the uncertainty as to the distance between respective actuator-sensor pairs for tubular structures would introduce additional complexity for determining the probability of damage presence defined by Eqs. (1) and (2). Without an appropriate configuration of the sensor network, the capability of the proposed algorithm for damage identification would be compromised. As indicated in Figs. 9(a)-(c), three possible unfolded forms with dissimilar configurations of actuator-sensor pairs are available for the tube specimen. All three configurations should be evaluated because of variation in the distance ratio defined by Eq. (2), although the correlation coefficients are identical for individual actuator-sensor pairs among the three cases.

Instead of using the raw wave signals, characteristic time points and corresponding amplitudes were extracted as principal wave components from individual raw wave signals and encapsulated using the concept of digital damage fingerprints (DDFs) (Lu *et al*. 2009) before and after the introduction of the damage in the experiments. The cross-correlation coefficients of DDFs between the damaged and benchmark structures were calculated for the 36 actuator-sensor pairs engaged, and are listed in Table 3. The lowest correlation coefficient for the hole of 11.9 mm diameter was 0.96 from the path of S3-S4, and the averaged values from typical paths of S1-S3, S4-S6 and S7-S9 were 0.994, 0.997 and 0.997. As a preliminary judgment, it was estimated that the damage should be located somewhere close to the area influenced by S3 and S4 for the lower values of correlation coefficients. The probability of the existence of damage was subsequently evaluated using Eq. (1) on a grid of 1×1 mm^2 meshed in the area enclosed by the sensor network.

With the configurations of actuator-sensor pairs shown in Figs. 9(a) and (b), Figs. 10(a) and (b) compare the predicted hole position which is marked by the symbol "+" with the actual hole position represented by the symbol "×". It is noted that the accuracy in identifying the position of damage was quite poor. In contrast, the probability of the presence of damage with the third configuration shown in Fig. 9(c) is shown in Figs. 11(a) and (b) for damage in the form of a hole of 9.0 mm and 11.9 mm diameter, respectively. The darkest circle indicates the area of the greatest possibility of the presence of damage with a threshold of 90%. The coordinates of the maximum value of probability, denoted as $P_{\max}$, represent

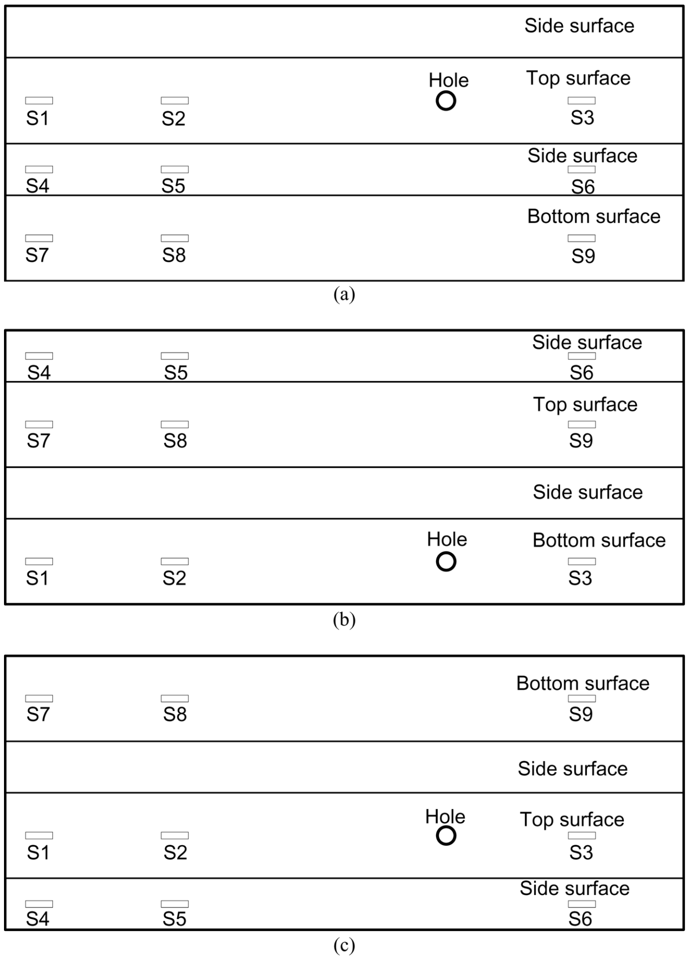

Fig. 9 Configurations of actuator-sensor pairs on the unfolded tube surface: (a) configuration 1, (b) configuration 2 and (c) configuration 3

Table 3 Actuator-sensor pairs for establishing probability of the presence of damage

Path	Path
S1 to S3 (S3 to S1)	S3 to S8 (S8 to S3)
S1 to S6 (S6 to S1)	S4 to S6 (S6 to S4)
S1 to S9 (S9 to S1)	S4 to S9 (S9 to S4)
S2 to S3 (S3 to S2)	S5 to S6 (S6 to S5)
S2 to S6 (S6 to S2)	S5 to S9 (S9 to S5)
S2 to S9 (S9 to S2)	S6 to S7 (S7 to S6)
S3 to S4 (S4 to S3)	S6 to S8 (S8 to S6)
S3 to S5 (S5 to S3)	S7 to S9 (S9 to S7)
S3 to S7 (S7 to S3)	S8 to S9 (S9 to S8)

the predicted central location of the damage. The predicted and actual centers of the damage for different hole sizes are compared in Table 4, in the coordinate system where the center of sensor S7

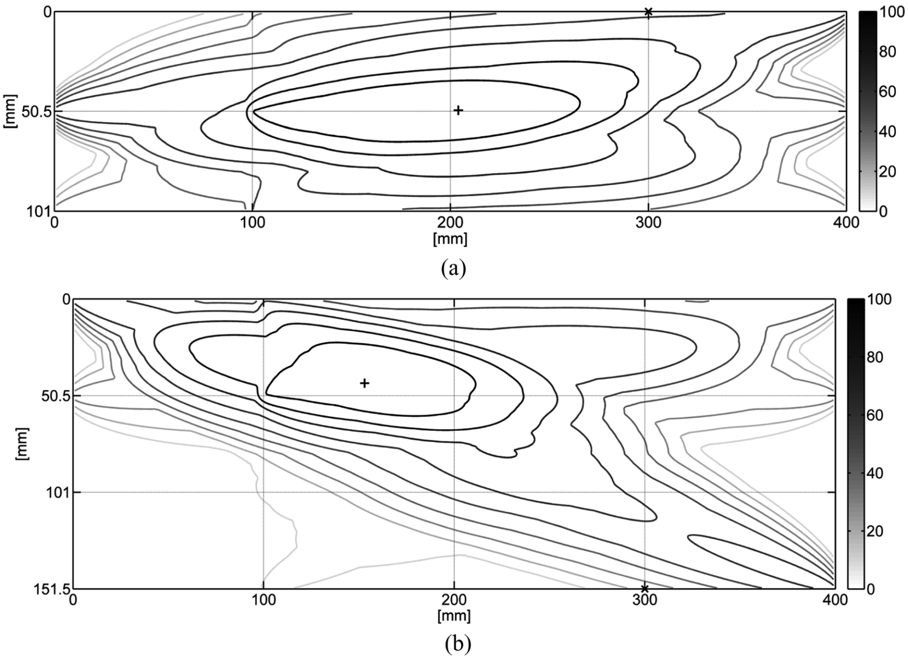

Fig. 10 Probability of the presence of damage: (a) configuration 1 and (b) configuration 2

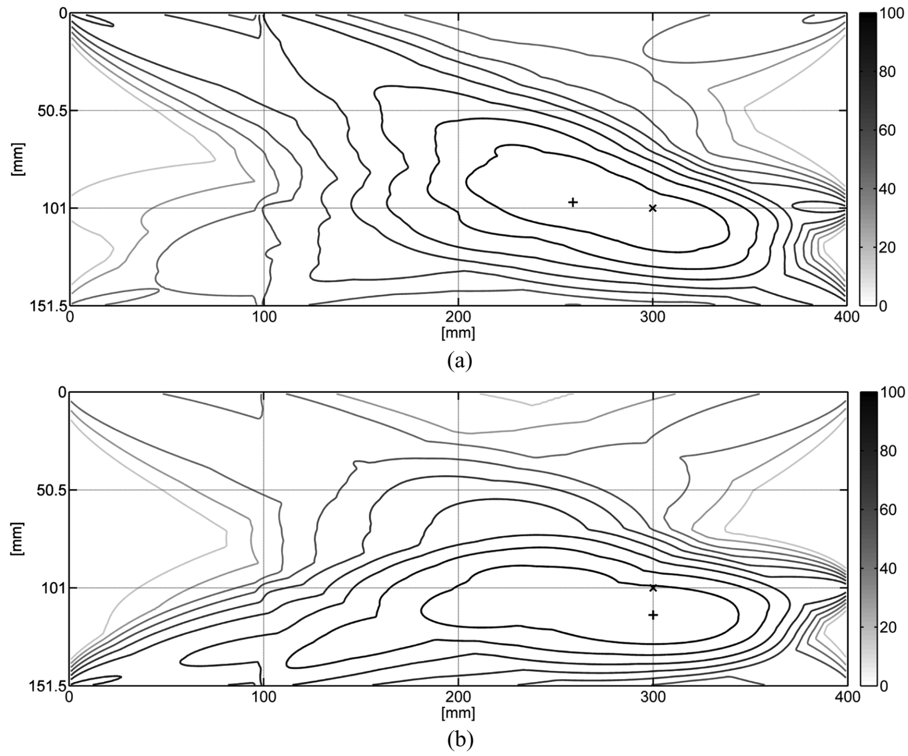

Fig. 11 Probability of the presence of damage with the third configuration of actuator-sensor pairs: (a) hole of 9.0 mm diameter and (b) hole of 11.9 mm diameter

Table 4 Comparison of predicted and actual hole positions

Diameter=3 mm	Diameter=4.6 mm	Diameter=9.0 mm	Diameter=10.5 mm	Diameter=11.9 mm
(399 mm, 101 mm)	(248 mm, 76 mm)	(259 mm, 98 mm)	(305 mm, 114 mm)	(300 mm, 115 mm)

*Actual position is (300 mm, 101 mm)

is the coordinate origin.

The main reason for the inaccuracy using the sensor configurations shown in Figs. 9(a) and (b) may be attributable to the fact that the damage was located at the edge of the sensor network, where fewer actuator-sensor paths contributed to the construction of the probability of the existence of damage. In contrast, the damage is encircled by the sensor network in the third configuration shown in Fig. 9(c). As a result, the number of sensitive actuator-sensor paths (paths that lie close to or exactly across the damage) increased considerably. The capability of the desired sensor network for locating the damage was therefore significantly enhanced.

It is also appreciated that different severities of damage will induce dissimilar energy distribution of wave signals. It is thus noticed that the accuracy of prediction improves with an increase in the severity of damage (that is, a larger hole), where more obvious deviation occurs or lower correlation to the benchmark is obtained, making identification easier. In particular, the identification accuracy for the smallest damage (the hole of 3 mm diameter) is exceptionally poor even with the third configuration, implying that the proposed approach may lack effectiveness for a hole of small diameter. On the other hand, the diagnosis results are almost the same for the holes of 10.5 and 11.9 mm in diameter, indicating that the precision of the proposed algorithm approached stability with the increase in the severity of damage, and the inaccuracy for the two larger holes may be attributable to system error in the experiments.

7. Conclusions

The propagation characteristics of piezo-activated guided waves in an aluminium tube of rectangular-section were investigated in this study using numerical simulations and experiments. Changes in propagating velocity and amplitude of the first wave packet that was recognized as L(0,2) mode were observed in the frequency range from 50 to 250 kHz. The wave scattering induced by through-thickness holes of different diameters was studied experimentally with the aid of an active sensor network. For the complex interaction between guided waves, damage, and structural boundaries, an algorithm based on correlation evaluation of wave signals was developed for the tubular structures. Different configurations of actuator-sensor pairs for tubular structures were developed for the purpose of precisely locating the position of the damage.

It was concluded that guided waves demonstrate diverse propagation properties in the frequency range of interest. The propagation of L(0,2) mode in the current tubular structure, which is similar to the performance of the S_0 mode in plate-like structures, demonstrated the maximum magnitude with less dispersion at a central frequency of 100 kHz. More energy loss occurs when guided waves propagate along the surfaces of the rectangular-section tube, which introduces more difficulty for signal processing and identification. Although guided waves propagate helically in clockwise and counter-clockwise directions, L(0,2) mode remained sensitive to damage even when it was not on the surface where the actuators and sensors were attached. The proposed approach can intuitively establish the probability of the presence of damage with good estimation of its location. The proposed algorithm is a promising method to effectively detect the position of damage, eliminating the need to extract ToF information from complex signal segments, which is the prerequisite for most forward analyses.

Acknowledgements

Y. LU is grateful for the support from the State Key Laboratory of Mechanical System and Vibration, Shanghai Jiao Tong University (VSN-2008-05). The authors are also grateful for the Hong Kong Polytechnic University Research Grant G-U204 and Research Grant Council of the Hong Kong Special Administration Region (project no. PolyU5333/07E). Y. LU and L. YE are also grateful for the research support of the Australian Postdoctoral Fellowship (ARC-APD) and a Discovery Project (DP) from the Australian Research Council.

References

Alleyne, D.N., Pavlakovic, B., Lowe, M.J.S. and Cawley, P. (2001), "Rapid long-range inspection of chemical plant pipework using guided waves", *Insight*, **43**, 93-96.

Castaings, M. and Hosten, B. (2001), "The propagation of guided waves in composite, sandwich-like structures and their use for NDT", *Rev. Prog. Quant. Nondest. Eval.*, **20**, 999-1006.

Cawley, P. and Alleyne, D. (1996), "The use of Lamb waves for the long range inspection of large structures", *Ultrasonics*, **34**(2-5), 287-290.

Dalton, R.P., Cawley, P. and Lowe, M.J.S. (2001), "The potential of guided waves for monitoring large areas of metallic aircraft fuselage structure", *J. Nondestruct. Eval.*, **20**(1), 29-46.

Demma, A., Cawley, P., Lowe, M.J.S. and Roosenbrand, A.G. (2003), "The reflection of the fundamental torsional mode from cracks and notches in pipes", *J. Acoust. Soc. Am.*, **114**(2), 611-625.

Demma, A., Cawley, P., Lowe, M.J.S., Roosenbrand, A.G. and Pavlakovic, B. (2004), "The reflection of guided waves from notches in pipes: a guide for interpreting corrosion measurements", *NDT&E Int.*, **37**(3), 167-180.

Diligent, O., Grahn, T., Boström, A., Cawley, P. and Lowe, M.J.S. (2002), "The low-frequency reflection and scattering of the S_0 Lamb mode from a circular through-thickness hole in a plate: finite element, analytical and experimental studies", *J. Acoust. Soc. Am.*, **112**(6), 2589-2601.

Giurgiutiu, V., Zagrai, A.N., Bao, J.J., Redmond, J.M., Roach, D. and Rackow, K. (2003), "Active sensors for health monitoring of aging aerospace structures", *Int. J. Condition Monit. Diagnostic Eng. Manag.*, **6**, 3-21.

Giurgiutiu, V. and Cuc, A. (2005), "Embedded non-destructive evaluation for structural health monitoring, damage detection, and failure prevention", *Shock Vib. Digest*, **37**(2), 83-105.

Grondel, S., Delebarre, C., Assaad, J., Dupuis, J.P. and Reithler, L. (2002), "Fatigue crack monitoring of riveted aluminium strap joins by Lamb wave analysis and acoustic emission measurement techniques", *NDT&E Int.*, **35**(3), 137-146.

Hay, T.R., Royer, R.L., Gao, H.D., Zhao, X. and Rose, J.L. (2006), "A comparison of embedded sensor Lamb wave ultrasonic tomography approaches for material loss detection", *Smart Mater. Struct.*, **15**(4), 946-951.

Hesse, D. and Cawley, P. (2006), "Surface wave modes in rails", *J. Acoust. Soc. Am.*, **120**(2), 733-740.

Lanza di Scalea, F., Matt, H. and Bartoli, I. (2007), "The response of rectangular piezoelectric sensors to Rayleigh and Lamb ultrasonic waves", *J. Acoust. Soc. Am.*, **121**(1), 175-187.

Leonard, K.R. and Hinders, M.K. (2003), "Guided wave helical ultrasonic tomography of pipes", *J. Acoust. Soc. Am.*, **114**(2), 767-774.

Lowe, M.J.S., Alleyne, D.N. and Cawley, P. (1998), "Defect detection in pipes using guided waves", *Ultrasonics*, **36**(1-5), 147-154.

Lowe, M.J.S. (1998), "Characteristics of the reflection of Lamb waves from defects in plates and pipes", *Rev. Prog. Quant. Nondest. Eval.*, **17**, 113-120.

Lu, Y., Ye, L., Su, Z. and Huang, N. (2007), "Quantitative evaluation of crack orientation in aluminium plates based on Lamb waves", *Smart Mater. Struct.*, **16**, 1907-1914.

Lu, Y., Ye, L., Su, Z. and Yang, C. (2008), "Quantitative assessment of through-thickness crack size based on Lamb wave scattering in aluminium plates", *NDT&E Int.*, **41**(1), 59-68.

Lu, Y., Ye, L., Wang, D. and Zhong, Z.R. (2009), "Time-domain analyses and correlations of Lamb wave signals for damage detection in a composite panel of multiple stiffeners", *J. Compos. Mater.*, **43**(26), 3211-3230.

Monnier, T. (2006), "Lamb waves-based impact damage monitoring of a stiffened aircraft panel using piezoelectric transducers", *J. Intel. Mat. Syst. Str.*, **17**(5), 411-421.

Park, M.H., Kim, I.S. and Yoon, Y.K. (1996), "Ultrasonic inspection of long steel pipes using Lamb waves", *NDT&E Int.*, **29**(1), 13-20.

Pei, J., Yousuf, M.I., Degertekin, F.L., Honein, B.V. and Khuri-Yakub, B.T. (1996), "Lamb wave tomography and its application in pipe erosion/corrosion monitoring", *Res. Nondestruct. Eval.*, **8**(4), 189-197.

Pu, S.H., Cegla, F., Drozdz, M., Lowe, M.J.S., Cawley, P. and Buenfeld, N.R. (2004), "Monitoring the setting and early hardening of concrete using an ultrasonic waveguide", *Insight*, **46**(6), 350-354.

Rizzo, P. and Lanza di Scalea, F. (2006), "Wavelet-based feature extraction for automatic defect classification in strands by ultrasonic structural monitoring", *Smart Struct. Syst.*, **2**(3), 253-274.

Rose, J.L. (1999), *Ultrasonic Waves in Solid Media*, Cambridge University Press, Cambridge, New York.

Silk, M.G. and Bainton, K.F. (1979), "The propagation in metal tubing of ultrasonic wave modes equivalent to Lamb waves", *Ultrasonics*, **17**(1), 11-19.

Thwaites, S. and Clark, N.H. (1995), "Non-destructive testing of honeycomb sandwich structures using elastic waves", *J. Sound Vib.*, **187**(2), 253-269.

Tua, P.S., Quek, S.T. and Wang, Q. (2005), "Detection of cracks in cylindrical pipes and plates using piezoactuated Lamb waves", *Smart Mater. Struct.*, **14**, 1325-1342.

Valle, C., Niethammer, M., Qu, J.M. and Jacobs, L.J. (2001), "Crack characterization using guided circumferential waves", *J. Acoust. Soc. Am.*, **110**(3), 1282-1290.

Wang, D., Ye, L. and Lu, Y. (2009), "A probabilistic diagnostic algorithm for identification of multiple notches using digital damage fingerprints (DDFs)", *J. Intel. Mat. Syst. Str.*, **20**(12), 1439-1450.

Zhang, L., Gavigan, B.J. and Rose, J.L. (2006), "High frequency guided wave natural focusing pipe inspection with frequency and angle tuning", *J. Press. Vess.-T. ASCE*, **128**(3), 433-438.

Zhao, X., Gao, H.D., Zhang, G.F., Ayhan, B., Yan, F., Kwan, C. and Rose, J.L. (2007) "Active health monitoring of an aircraft wing with embedded piezoelectric sensor/actuator network: I. Defect detection, localization and growth monitoring", *Smart Mater. Struct.*, **16**(4), 1208-1217.

Zhou, L., Yuan, F.G. and Meng, W.J. (2007), "A pre-stack migration method for damage identification in composite structures", *Smart Struct. Syst.*, **3**(4), 439-454.

CC